03

Flow structure and heat transfer in a gas-droplet flow behind a sudden channel constriction

© M.A. Pakhomov, V.I. Terekhov

Kutateladze Institute of Thermophysics, Siberian Branch, Russian Academy of Sciences,
Novosibirsk, Russia
e-mail: pma41976@yandex.ru; terekhov@itp.nsc.ru

Received February 14, 2023
Revised March 22, 2023
Accepted April 2, 2023

The numerical study of the local flow structure and heat transfer in a gas-droplet turbulent flow behind a forward-facing step in the two-phase gas-droplet flow is carried out. Two-dimensional steady-state Reynolds-averaged Navier-Stokes (RANS) equations are used for the numerical solution. They were written taking into account the presence of a dispersed phase. The Eulerian two-fluid approach is used to describe the flow dynamics and heat and mass transfer in the gaseous and dispersed phases. The turbulence of the carrier phase was described using an elliptical model for the transport of Reynolds stress components, taking into account the presence of droplets. The effect of evaporating droplets flowing after the forward-facing step on the local flow structure, turbulence, distribution of the dispersed phase, and heat transfer inetensification is analyzed.

Keywords: numerical simulation, Reynolds stress transport model, turbulence, heat transfer.

DOI: 10.61011/TP.2023.06.56524.23-23

Introduction

The problem of heat transfer intensification continues to be one of the most urgent in modern technology. The control of the flow structure and heat transfer in fluid flows is implemented using active (for example, imposition of flow pulsations, etc.) and passive (for example, heat transfer intensifiers, etc.) methods. Passive methods of flow and heat exchange control are simpler and more reliable than active ones. Passive heat exchange intensifiers are placed on the protected surfaces of the flow part of the working channels and have the form of protrusions and (or) recesses of various configurations [1–4]. The examination of influence of shapes and locations of the protrusions located on the surface of a flat channel or a pipe on the flow structure and the heat transfer to study both forced [1–4] and free [5] convection of a single-phase liquid is important in this context. By definition such flows can be divided into two groups. The first one is the flow after the backward-facing step (BFS) and the second one is forward-facing step (FFS). The case of flow and heat transfer in the flow of the single-phase fluid behind the BFS was studied much better. Let us note some monographs [3,4,6] and review papers [7–9] on this topic.

A one- or two-phase flow in the flat channel behind the FFS has two pronounced vortex (separation) domains immediately before and behind the flow narrowing cross-section (Fig. 1). Separation of the two-phase flow before the sudden narrowing cross-section, the formation of sections of flow recirculation (before and behind the sudden narrowing of the flow) and its subsequent reattachment behind the forward-facing step are often encountered when flowing after the airfoil and heat-power equipment elements. In this case, significant changes in the averaged velocity, turbulence, pressure, and heat transfer are observed in the vicinity of separation. The case of flowing behind the forward-facing step is more complicated then flow past BFS due to the presence of two domains of flow recirculation that are formed when it is separated (Fig. 1) [10 –12]. The boundary layer detaches from the surface on approach to a forward-facing step. The length of this small flow separation domain is $x_{R1} = (1 - 1.5)h$ [12], where h is the step height. Beyond a sudden narrowing of the channel, a domain of flow separation from its sharp edge forms. The length of this domain is normally several times greater than the step height: $x_{R2} = (1.7 - 4)h$ [12].

Previously, experimental and numerical studies of the evaporation of atomized finely dispersed liquid droplets in flows behind a sudden expansion of the channel [13,14] were executed, for a finned flat channel [15] or a pipe [16,17]. These studies show that the use of the latent heat of phase transition leads to a noticeable increase in heat transfer (by several times in comparison with a single-phase flow under other identical conditions) in comparison with traditional forced convection in a single-phase flow. So, note that very few studies focused on the flow structure and the heat transfer in a turbulent two-phase flow upon presence of evaporating droplets flowing behind two-dimensional obstacles (backward-facing steps and two-dimensional obstacles of other shapes) have been published [13–17].

We have already performed detailed numerical studies of the flow structure, turbulence, and the heat transfer in separation gas-droplet flows behind the flat backward-facing step [14], and a sudden expansion of the pipe [16,17]. The validity of the numerical code used in these studies was

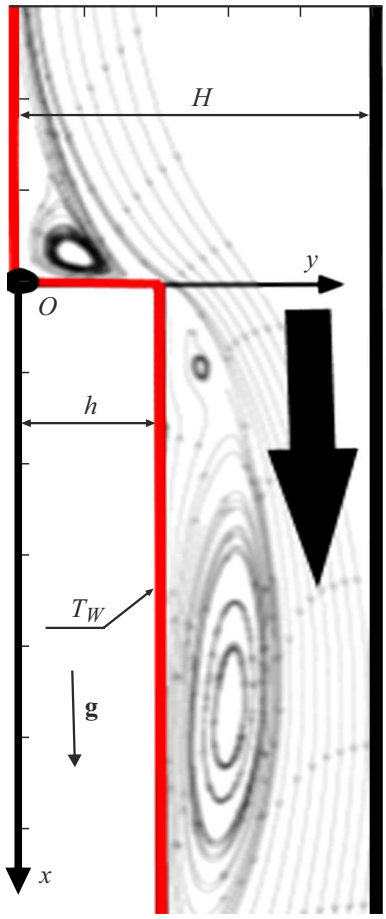

Figure 1. Scheme of gas-droplet flow flowing after the forward-facing step. The arrow designates a direction of movement of the gas-droplet flow. Wall with heated surface is shown in red (in on-line version).

verified by comparing the results with measurement data on the flow structure and the heat transfer for the gas-droplet flow behind the backward-facing step [13]. As far as we know, the gas-droplet flow flowing after the forward-facing step were not studied yet. In the present study the influence of the sudden narrowing of the flat channel on the local structure of the turbulent flow and the heat transfer in the separation gas-droplet flow with evaporating droplets is examined numerically. Note that this paper is a logical continuation and extended version of the paper [18].

1. Mathematical model

The system of equations for modeling the motion of the dispersed phase in the Eulerian continuum representation is obtained from the kinetic equation for the probability density function of particle distribution in the turbulent flow [19]. The problem of dynamics of a two-phase gas-droplet turbulent flow with an interphase heat transfer flowing past a flat forward-facing step (Fig. 1) is considered. Two-dimensional steady-state RANS (Reynolds-averaged Navier-Stokes) equations written with account for the influence of particles on transport processes in gaseous phase [14] are used to solve this problem. The Eulerian continuum approach is applied to characterize the dynamics of flow and heat-and-mass transfer in gaseous and disperse phases.

$$\rho\frac{\partial U_j}{\partial x_j}=\frac{6J}{d}\Phi,$$

$$\frac{\partial(U_iU_j)}{\partial x_i}=-\frac{\partial P}{\rho\partial x_i}+\frac{\partial}{\partial x_j}\left(\nu\frac{\partial U_i}{\partial x_j}-\langle u_i'u_j'\rangle\right)$$

$$-(U_i-U_{Li})\frac{M_L}{\tau},$$

$$\frac{(\partial U_iT)}{\partial x_i}=\frac{\partial}{\partial x_i}\left(\frac{\nu}{\mathrm{Pr}}\frac{\partial T}{\partial x_i}-\langle u_j't\rangle\right)+D_T\frac{(C_{PV}-C_{PA})}{C_P}$$

$$\times\left(\frac{\partial K_V}{\partial x_i}\frac{\partial T}{\partial x_i}\right)-\frac{6\Phi}{\rho C_Pd}[\alpha(T-T_L)+JL], \qquad (1)$$

$$\frac{\partial(U_iK_V)}{\partial x_i}=\frac{\partial}{\partial x_i}\left(\frac{\nu}{\mathrm{Sc}}\frac{\partial K_V}{\partial x_i}-\langle u_j'k_V\rangle\right)+\frac{6J\Phi}{d},$$

$$\rho=P/(R_gT).$$

Here $U_i(U_x\equiv U,\ U_y\equiv V)$, u_i' $(u_x'\equiv u',\ u_y'\equiv v')$ — components of the average velocity of the carrier phase and its pulsation, x_i — projections on the coordinate axes, $\langle u', u_i'\rangle$ — Reynolds stresses, $\tau=\rho_Ld^2/(18\mu W)$ — particle dynamic relaxation time, written taking into account the deviation from the Stokes flow law, $W=1+0.15\mathrm{Re}_L^{0.687}$, $\mathrm{Re}_L=|\mathbf{U}_S-\mathbf{U}_L|d_1/\nu$ — Reynolds number of the dispersed phase, constructed from the interfacial velocity, $\mathbf{U}_S$ and $\mathbf{U}_L$ — vectors of the actual velocity of the gaseous phase at the location of the particle [20] and droplets, respectively. Turbulent heat and diffusionsl fluxes in the gaseous phase are determined according to the Boussinesq hypothesis. For turbulent Prandtl and Schmidt numbers $\mathrm{Pr}_T=\mathrm{Sc}_T=0.9$ is accepted.

$$\langle u_j't\rangle=-\frac{\nu_T}{\mathrm{Pr}_T}\frac{\partial T}{\partial x_j},\quad \langle u_j'k_V\rangle=-\frac{\nu_T}{\mathrm{Sc}_T}\frac{\partial K_V}{\partial x_j}. \qquad (2)$$

All equations of system (1) are written taking into account the presence and influence of the dispersed phase evaporation on the transport processes of momentum, heat, and mass in the gas flow. The system of averaged equations describing the transport processes in the dispersed phase has the following form:

$$\frac{\partial(\rho_L\Phi U_{Lj})}{\partial x_j}=-\frac{6J\Phi}{d},$$

$$\frac{\partial(\rho_L\Phi U_{Lj}U_{Li})}{\partial x_j}+\frac{\partial(\rho_L\Phi\langle u_{Li}u_{Lj}\rangle)}{\partial x_j}=\Phi(U_i-U_{Li})\frac{\rho_L}{\tau}$$

$$+\Phi\rho_Lg-\frac{1}{\tau}\frac{\partial(\rho_LD_{Lij}\Phi)}{\partial x_j}-\frac{\partial(\Phi P)}{\partial x_i}, \qquad (3)$$

$$\frac{\partial(\rho_L \Phi U_{Lj} T_L)}{\partial x_j} + \frac{\partial}{\partial x_j}(\rho_L \Phi \langle \theta u_{Lj} \rangle)$$

$$= \Phi(T - T_L)\frac{\rho_L}{\tau_\Theta} - \frac{\mathbf{1}}{\tau_\Theta}\frac{\partial(\rho_L D^\Theta_{Lij}\Phi}{\partial x_j}.$$

Here D_{Lij}, $D^\Theta_{L,ij}$ — tensors of turbulent diffusion and turbulent heat transfer of the dispersed phase [19]; $\tau_\Theta = C_{PL}d^2/(12\lambda Y)$ — droplets thermal relaxation time, $Y = 1 + 0.3\mathrm{Re}_L^{1/2}\mathrm{Pr}^{1/3}$; C_{PL}, ρ_L — heat capacity and material density of droplets.

The system of equations (3) takes into account the change in the amplitude of fluctuations in the velocity and concentration of the dispersed phase both in the longitudinal and transverse directions. The significant nonisotropy of the amplitudes of turbulent fluctuations of particle velocity is taken into account. The equations do not take into account the thermophoresis of dispersed phase droplets, the Magnus and Saffman forces due to small value of these force factors in comparison with those taken into account in this paper. The radial movement of droplets is caused by convection, viscous friction force, turbophoresis force (turbulent migration) due to the heterogeneity of the turbulent energy of the dispersed phase, as well as turbulent diffusion of the dispersed phase associated with their concentration gradient. The coefficients of turbulent diffusion of the dispersed phase in the momentum equations of the system (3) are due to the chaotic motion of droplets and their involvement by energy-intensive vortices of the carrier phase and, are determined by the model [19].

Equations for calculating the second moments of fluctuations of the dispersed phase velocity $\langle u'_{Li}u'_{Lj}\rangle$, temperature $\langle \theta'^2_{Lj}\rangle$ and turbulent heat flux $\langle \theta u_{Lj}\rangle$ are given in [19]. The second moments of fluctuations of the dispersed impurity velocity in the longitudinal and transverse directions take into account the involvement of particles in turbulence as a result of the action of viscous forces, convective and diffusion transfers, as well as an increase in the intensity of the pulsating motion of the dispersed phase in the longitudinal direction due to the generation of turbulence from the average motion. The turbulent heat flux in the dispersed phase is due to the particles involvment in the fluctuations of the velocity and temperature of the gas, and the heat transfer as a result of the chaotic motion of droplets. The intensity of particle temperature fluctuations is determined by heat transfer between the continuous medium and particles, convective transfer, turbulent diffusion of heat, as well as the generation of temperature fluctuations as a result of non-isothermal flow.

Turbulence of the carrier phase is described using the elliptical model for the transport of Reynolds stress components [21] written taking into account the two-phase nature of the flow [19]. The basic equations of the model [14] are given in [17], but not here. The particles effect on the carrier phase due to pulsating interfacial slip has the form [19]:

$$A_L = \frac{2\rho_L\Phi}{\rho\tau}(1 - f_u)\langle u_i u_i\rangle, \quad \varepsilon_L = \frac{2\rho_L\varepsilon\Phi}{\rho\tau}(1 - f_\varepsilon), \quad (4)$$

where f_u and f_ε — coefficients characterizing the particles involvement in the turbulent motion of gas [19]. The functions f_u and f_ε are determined by the time of the droplet contact with the energy-intensive vortices of the carrier phase [19]. The constants and functions of the turbulence model are given in [21]. The redistributing term describes the energy exchange between the individual components of the Reynolds stress components due to the correlation pressure–strain rate. It is written taking into account the influence of the two-phase flow [22]. The system of equations (1) –(4) is supplemented by the heat transfer equation at the interface, provided that the temperature is constant along the droplet radius, and by the equation of vapor mass conservation on its evaporating surface [16].

The schematic flow diagram is presented in Fig. 1. The volume concentration of droplets is low ($\Phi_1 = M_{L1}\rho/\rho_L < 2 \cdot 10^{-4}$), and they are rather small (initial diameter $d_1 \le 20\,\mu$m). Here M_{L1} — initial mass concentration of droplets, ρ and ρ_L — density of gas and droplets. Therefore, the breakup and coalescence of droplets in a flow are neglected [14,16,17].

2. Numerical implementation

A numerical solution was obtained using the finite-volume method on a structured grid. The authors Eulerian in-house code was used to find this solution. For the convective terms of differential equations, the QUICK (Quadratic before Interpolation for Convective Kinematics) [23] procedure of the second order of accuracy was used. Central differences of the second order of accuracy were used for diffusion flows. The pressure field was corrected using the SIMPLEC (Semi-Implicit Method for Pressure Linked Equations-Consistent) finite-volume consistent procedure [24]. All calculations were performed on a „base“ grid containing 400×100 control volumes (CVs). The length of the calculation section before of the sudden channel narrowing was $5h$, and behind the narrowing it was $10h$ long. In order to verify the obtained independent solution from the number of computational cells, calculations were carried out on „coarse“ 200×50 and „fine“ 600×150 grids. The difference in calculated data on the turbulent kinetic energy of the carrier phase and the Nusselt number between the base and „fine“ grids was below 0.1%. Calculations were performed on the grid with clustering towards all solid surfaces and in flow recirculation domains. To resolve the mean flow field and turbulent characteristics of the two-phase flow in a viscous sublayer ($y_+ < 10$), at least 10 CVs were used, and the first computational node was located at a distance from any of the walls $y_+ \le 1$.

We already compared the calculated data with the results of experiments [25] with a two-phase turbulent flow of gaseous with solid particles flowing past a backward-facing step without heat transfer. These data were reported

in [14,17] and are not presented here. For comparison with the measurement data for the gas-droplet flow behind the flat BFS the measurement data in [13] were used. The satisfactory agreement with measurement data [13,25]. This was used as a basis for numerical modeling of the gas-droplet flow flowing after forward-facing step.

3. Results of numerical calculations and their analysis

All numerical calculations were performed for a monodisperse gas-droplet mixture at the duct inlet and for the case of a downward flow. The channel height before of the sudden narrowing is $H = 60$ mm, step height is $h = 20$ mm, and channel narrowing ratio is $\mathrm{ER} = (H - h)/H = 2/3$ (Fig. 1). The origin of coordinates corresponds to the cross section of sudden constriction of a two-phase flow. The mass-averaged velocity of gas before of the separation cross section is $U_{m1} = 5$ m/s, and the Reynolds number for the gas phase is $\mathrm{Re} = hU_{m1}/\nu = 6.7 \cdot 10^3$ and $\mathrm{Re}_H = HU_{m1}/\nu = 2 \cdot 10^4$. Water droplets are added to a single-phase air flow in the inlet cross section of the computational domain (i.e., at a distance of $5h$ from the cross section of sudden narrowing of the two-phase flow), and their initial velocity $U_{L1} = 0.8U_{m1}$ does not vary over the channel height. The initial mass fraction of water droplets $M_{L1} = 0{-}0.1$ and vapor $M_{V1} = 0.005$. The diameter of water droplets in the inlet cross section is $d_1 = 20\,\mu$m. Stokes number in averaged motion is $\mathrm{Stk} = \tau/\tau_f$, where $\tau_f = 5h/U_{m1}$ — characteristic turbulent scale [13,25]. The expression for τ_f is used for both the flow behind the flat backward-facing step [15] and sudden pipe expansion [16,17]. At $\mathrm{Stk} \ll 1$ the particles are involved in the separation motion of the gaseous phase, and at $\mathrm{Stk} > 1$ the dispersed phase does not participate in the recirculation motion [13,25]. The temperatures of air and droplets at the inlet are $T_1 = T_{L1} = 293$ K. The temperature of the wall with step was equal to $T_W = \mathrm{const} = 373$ K, and the opposite smooth wall was thermally insulated. The results of preliminary calculations for a single-phase flow in a flat duct with height H and length of $75H$ were used to set the input distributions of parameters of the gas flow. Thus, a completely hydrodynamically stabilized flow of the single-phase gas (air) flow is present at the inlet cross section of the computational domain.

The structure of a turbulent two-phase flow is altered substantially in flowing past a forward-facing step (Fig. 1). The main flow recirculation zone (behind a sudden duct constriction) extends for $x_{R1} \approx 3h$, and the recirculation zone upstream of the step is $x_{R2} \approx 1.1h$ in length. The flow reattaches to the end wall of the step at $y \approx -0.3h$. The positions of flow detachment and reattachment points were identified by zero longitudinal and transverse velocities of the carrier flow. The positions of flow recirculation centers for a vortex upstream of the step and the main vortex after the step are $(-0.3h, -0.2h)$ and $(0.8h, 0.15h)$, respectively. These conclusions agree qualitatively with the results of measurements [12,26] and calculations [11,27] for a single-phase flow past a FFS.

Fig. 2 shows the transverse profiles of the averaged longitudinal (a) and transverse (b) components of velocity, turbulence (c) and temperatures (d) in the single-phase flow $(M_{L1} = 0)$, as well as for the gas phase and droplets for the two-phase flow in six cross-sections before and behind the forward-facing step.

The profiles of the averaged longitudinal and transverse velocity components of the gaseous and dispersed phases are similar to those for the single-phase flow mode (Fig. 2, *a, b*). The gas velocity in the gas-droplet flow is slightly ($\leq 3\%$) ahead of the single-phase flow velocity. Due to its inertia, the particle velocity is higher than the corresponding value for the gas velocity in two-phase flow in almost the entire computational domain, except for a small area at $x/h \leq 1$. This is explained by the fact that low-inertia droplets at small Stokes numbers ($d_1 = 20\,\mu$m, $\mathrm{Stk} = 0.06$) are involved in the averaged motion of the gaseous phase and rise above the step, behind which they gradually accelerate. Thus, note that low-inertia droplets present in the entire computational domain, and they intensify heat transfer during their evaporation behind the sudden narrowing cross-section of the flow. In this case, there are two domains with a negative value of the longitudinal velocity of the gaseous phase, they locate before and behind the sudden narrowing of the channel. The maximum positive value is $U/U_{m1} = 2$, and it occurs behind the sudden narrowing of the channel at $x/h > 1$ and $y/h > 1$. The maximum value of the negative longitudinal velocity of gas in the single- and two-phase flow in the recirculation zone behind the step is $U/U_{m1} = -0.25$ and -0.2 for the vortex domain in before the step. This agrees qualitatively with the data from [14] obtained by DNS method.

The maximum positive value of the averaged transverse velocity component was obtained before of the leading edge of the step at $x/h = 0$ and $y/h = 0.5$ (Fig. 2, *b*). Negative values of the transverse velocity are observed in the flow recirculation domain. The peak value of the positive value of the speed is $V/U_{m1} = 0.6$, and the largest negative value is $V/U_{m1} = -0.1$ at $x/h = 1$ and $y/h = 0.2$.

Transverse distributions of the turbulent kinetic energy (TKE) of the carrier phase for the two-phase gas-droplet flow reveal that the TKE value in the mixing layer is the highest (Fig. 2, *c*). The turbulent kinetic energy for the two-dimensional flow was determined by the formula

$$2k = \langle u_i' u_i' \rangle = u'^2 + v'^2 + w'^2$$
$$\approx u'^2 + v'^2 + 0.5(u'^2 + v'^2) \approx 1.5(u'^2 + v'^2).$$

The turbulent kinetic energy increases on approach to the duct constriction. The maximum turbulence of the gaseous phase was found in the mixing layer and at $x/h \approx 2$. The turbulence value decreases on approach to the reattachment point. Turbulization of the flow in this cross section is associated with separation flow past a forward-facing step.

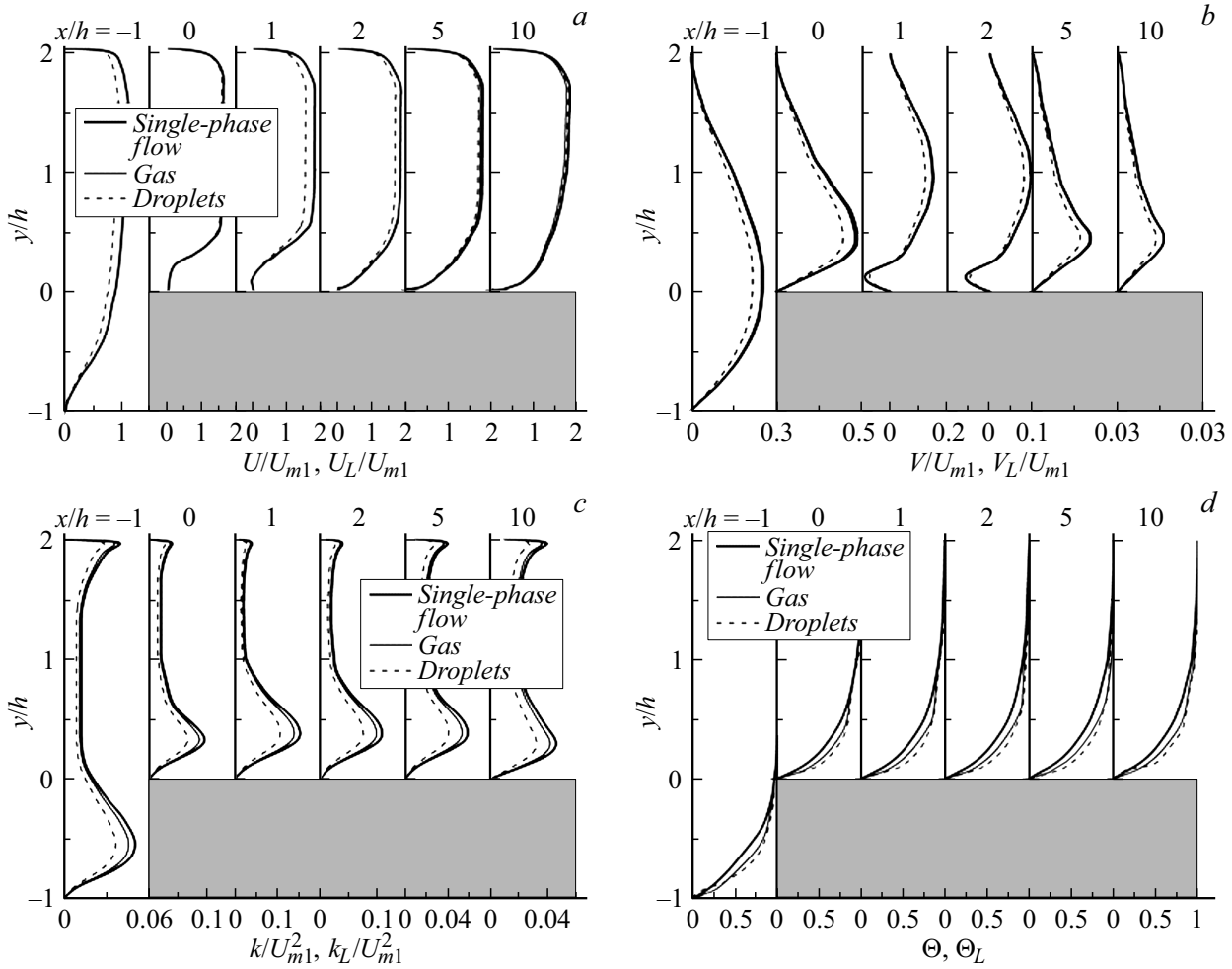

Figure 2. Profiles of the averaged longitudinal (a) and transverse (b) velocity components, turbulent kinetic energy (c) and temperatures (d) in the single-phase flow ($M_{L1} = 0$, thick continuous lines), carrier (thin continuous lines) and dispersed (dotted line) phases at $M_{L1} = 0.05$ along the longitudinal coordinate after the sudden narrowing of the flat channel. The gray rectangle represents the channel behind its sudden narrowing. $\mathrm{Re}_H = 2 \cdot 10^4$, $\mathrm{Re} = 6.7 \cdot 10^3$, $d_1 = 20\,\mu$m, $\mathrm{Stk} = 0.06$.

This holds true for both single-phase and two-phase flows. The TKE distributions of the carrier (thin continuous lines) and dispersed (dotted line) phases in the gas-droplet flow have the form similar to that for the single-phase flow (continuous line) in the flow separation domain. Note that the suppression of turbulence level of the gaseous phase is obtained when evaporating water droplets are added to the flow (up to 15%). The turbulent energy of water droplets remains lower than the corresponding value for the gaseous phase throughout the entire length of the computational domain, but also reaches its maximum at $x/h = 1-2$. This indicates the involvement of liquid droplets in the gaseous motion and their interaction with turbulent vortices of the gaseous phase.

The dimensionless temperatures of the phases are shown in Fig. 2, d, where $\Theta = (T_W - T)/(T_W - T_{1,m})$ and $\Theta_L = (T_{L,\max} - T_L)/(T_{L,\max} - T_{L1})$ are the dimensionless temperatures of the carrier phase and water droplets. Here $T_{L,\max}$ and $T_{L1,m}$ is the maximum temperature in the given cross-section and the droplet temperature in the inlet cross-section. It can be seen that the relative temperature profiles of single-phase and two-phase flows have qualitatively similar form. The gas temperature in the two-phase flow has a lower value (up to 20%) and, therefore, a more filled form in comparison with the corresponding profile for the single-phase flow due to the evaporation of droplets. This causes the intensification of heat transfer in the gas-droplet flow in comparison with the corresponding single-phase flow. The droplets temperature has the smallest value for all data of calculations shown in Fig. 2, d.

Fig. 3 shows the calculated profiles of the mass concentration of the dispersed phase along the channel length before and behind the cross-section of its sudden narrowing. The calculations were performed for two droplet diameters $d_1 = 20$ and $50\,\mu$m, which corresponds to the Stokes numbers in the averaged motion $\mathrm{Stk} = 0.06$ and 0.4. Finely dispersed droplets at $\mathrm{Stk} = 0.06$ are observed over the entire cross-section of the channel behind the sudden narrowing

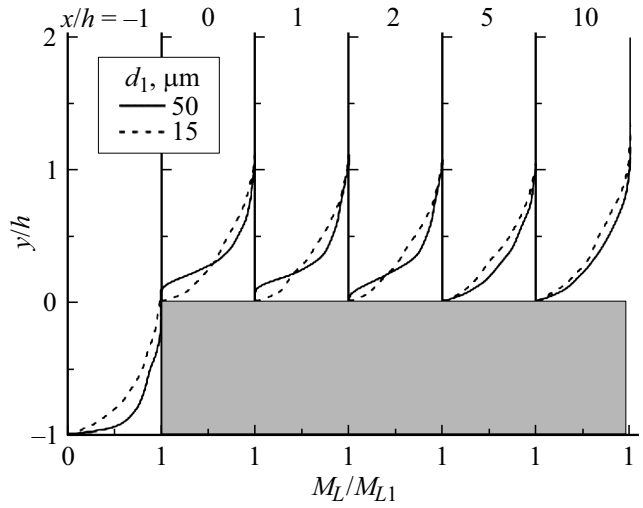

Figure 3. Influence of the initial droplet diameter on the distributions of the mass concentration of the dispersed phase. $\mathrm{Re}_H = 2 \cdot 10^4$, $\mathrm{Re} = 6.7 \cdot 10^3$, $M_{L1} = 0.05$.

and penetrate into the recirculation domains of the flow. It can be seen that with the initial size $d_1 = 50\,\mu$m they have large concentration in the vicinity of the FFS at $x/h = -1$. This is explained by the inertia of the dispersed phase. Also, droplets at $\mathrm{Stk} = 0.4$ practically do not penetrate into the domain of the main recirculation zone of the flow in the channel behind its sudden narrowing (cross-sections $x/h < 3$), and the droplets concentration in this region is $M_L/M_{L1} \approx 0$. They are observed only in the shear mixing layer and the flow core and penetrate into the near-wall part of the channel only after the two-phase flow reattachment point ($x/h > 3$).

The influence of the initial droplet diameter on the distributions of the local Nusselt number along the channel length is shown in Fig. 4. The Nusselt number is determined by the relation for the condition $T_W = \mathrm{const}$:

$$\mathrm{Nu} = -(\partial T/\partial y)_W h/(T_W - T_m),$$

where T_m — gas bulk temperature in the given cross-section. The addition of evaporating droplets to the separated single-phase flow leads to significant intensification of heat transfer (almost by 2 times) compared to the single-phase air flow when flowing after FFS. The heat transfer increase in comparison with a fully developed air flow in the flat channel at fixed Reynolds number for the case of the single-phase flow ($M_{L1} = 0$) in the flat channel exceeds 4 times for $M_{L1} = 0.05$ and $d_1 = 10\,\mu$m. The heat transfer intensification is observed both in the recirculation zone ($x_{R2}/h < 2.75$) and in the flow relaxation domain in comparison with the single-phase flow after the forward-facing step. As droplets evaporate and movement in the downward flow direction, the heat transfer intensity tends to the corresponding value for the single-phase stabilized flow in the flat channel behind its narrowing. The heat transfer maximum is located in the flow recirculation domain for FFS, while for the flow after BFS, the maximum heat transfer in a single-phase flow is located in the domain of its connection [3]. This is typical for both one- and two-phase flow modes with small droplets [14,16,17]. Under these conditions the length of the main separation domain is $x_{R2} = 2.75h$ and of the small separation zone before the step is $x_{R1} = 1.1h$.

The smallest droplets in the studied range ($d_1 = 10\,\mu$m and $\mathrm{Stk} \approx 0.02$) evaporate most intensively due to the larger area of the phase interface, but over a shorter pipe length. The greatest increase in heat transfer was obtained for fine dispersed water droplets at $\mathrm{Stk} \leq 0.02-0.03$. The increase in particle size impairs the droplets involvement in the recirculation movement due to the increase in the Stokes number, and complicates their rise and penetration into the channel after its sudden narrowing. This is confirmed by data in Fig. 3. For droplets with the initial diameter of $d_1 = 50\,\mu$m ($\mathrm{Stk} \approx 0.4$), it is shown that for them the area of interface contact is significantly reduced, and accordingly they intensify heat transfer worse and weakly penetrate into the main domain of flow separation located in channel behind its narrowing.

The effect of the Stokes number in the averaged motion on the heat transfer intensification parameter $\mathrm{Nu}_{\max}/\mathrm{Nu}_{\max,0}$ is shown in Fig. 5, where $\mathrm{Nu}_{\max,0}$ is the maximum Nusselt number for the single-phase flow after FFS. The calculation is made with a change in the Stokes number in the range $\mathrm{Stk} = 0-1.5$, which, according to [13,25], corresponds to the modes both with the particles involvement in the turbulent motion of the carrier phase, and with the absence of their involvement. With the increase in the droplet diameter, the decrease in the maximum value of heat transfer is observed. The increase in the initial mass concentration of droplets causes the increase in the transfer intensification parameter.

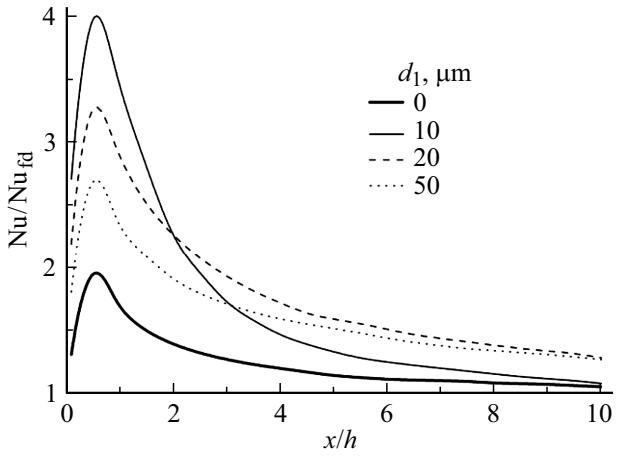

Figure 4. Heat transfer in the separation gas-droplet flow behind the sudden narrowing of flow under variation of initial diameter. $\mathrm{Nu}_{\mathrm{fd}} = 36$, $\mathrm{Re}_H = 2 \cdot 10^4$, $\mathrm{Re} = 6.7 \cdot 10^3$, $M_{L1} = 0.05$.

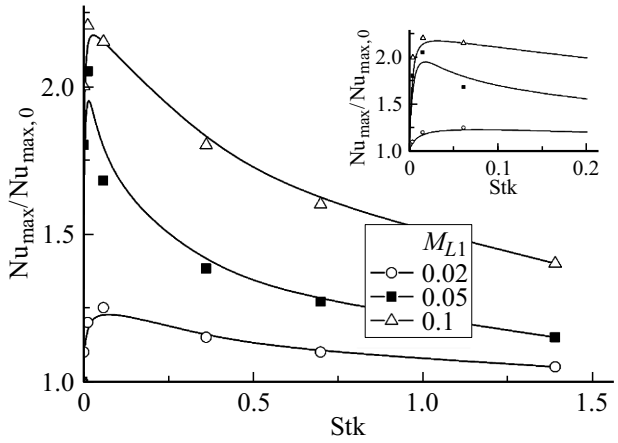

Figure 5. Influence of Stokes number in the averaged motion on the heat transfer intensification parameter.

Conclusion

In this paper the numerical study of the local flow structure and heat transfer in a gas-drop turbulent flow behind a forward-facing step in the two-phase gas-droplet flow is carried out. When solving, two-dimensional steady-state Reynolds-averaged Navier–Stokes (RANS) equations are used, written considering the presence of the dispersed phase. The Eulerian approach is applied to describe the flow dynamics and heat-and-mass transfer in gaseous and dispersed phases. Turbulence of the carrier phase is described using the elliptical model for the transport of Reynolds stress components written taking into account the two-phase nature of the flow.

The profiles of the averaged longitudinal and transverse velocity components of the gaseous and dispersed phases are similar to those for the single-phase flow mode. The suppression of turbulence level of the gaseous phase is obtained when evaporating water droplets are added to the flow (up to 15%). The turbulent energy of water droplets remains lower than the corresponding value for the gas phase throughout the entire length of the computational domain. Fine droplets ($Stk = 0.06$) are observed over the entire cross-section of the channel behind the sudden narrowing and penetrate into the flow recirculation domains, while more inertial particles at $\mathrm{Stk} = 0.4$ do not penetrate into the main flow recirculation domain. The addition of evaporating droplets to the separated single-phase flow behind its sudden narrowing leads to significant intensification of heat transfer (by more than 2 times) compared to the single-phase air flow under other conditions being equal. The change in the initial droplet diameter has a more complex effect on heat transfer in the two-phase flow behind the sudden narrowing of the channel. The smallest droplets at $\mathrm{Stk} \approx 0.02$ evaporate most intensively due to the larger area of the interface, but over shorter pipe length. The greatest increase in heat transfer was obtained for fine dispersed water droplets at $\mathrm{Stk} \leq 0.02-0.03$. The increase in particle size impairs the droplets involvement in the recirculation movement due to the increase in the Stokes number. Droplets of the largest initial diameter studied at $\mathrm{Stk} \approx 0.4$ intensify heat transfer worse and practically do not penetrate into the domain of the main flow recirculation in the channel behind the sudden narrowing.

Funding

Numerical calculations were supported financially by the Russian Science Foundation (grant No. 21-19-00162).

Conflict of interest

The authors declare that they have no conflict of interest.

References

[1] E.K. Kalinin, G.A. Dreitser, S.A. Yarkho. *Intensifikatsiya teploobmena v kanalakh* (Mashinostroenie, M., 1990))in Russian)
[2] Yu.F. Gortyshov, I.A. Popov, V.V. Olimpiyev, A.V. Shchelchkov, S.I. Kaskov. *Teplogidravlicheskaya effektivnost perspektivnykh sposobov intensifikatsii teplootdachi v kanalakh teploobmennogo oborudovaniya. Intensifikatsiya teploobmena* (Tsentr innovatsionnykh tekhnologiy, Kazan, 2009) (in Russian)
[3] V.I. Terekhov, T.V. Bogatko, A.Yu. Dyachenko, Ya.I. Smulsky, N.I. Yarygina. *Heat Transfer in Subsonic Separated Flows* (Springer, Cham, 2021)
[4] Yu.A. Bystrov, S.A. Isaev, N.A. Kudryavtsev, A.I. Leont'ev, *Chislennoe modelirovanie vikhrevoi intensifikatsii teploobmena v paketakh trub* (Sudostroenie, SPb., 2005) (in Russian).
[5] A.M. Levchenya, E.M. Smirnov, S.N. Trunova. Tech. Phys. Lett., **48** (3), 40, (2022). DOI: 10.21883/PJTF.2022.03.51984.19020
[6] V.E. Alemasov, G.A. Glebov, A.P. Kozlov. *Termoanemometricheskie metody issledovaniya otryvnykh techeniy* (Izd-vo Kazanskogi f-la AN sssR, Kazan, 1989) (in Russian)
[7] R.L. Simpson. Progress Aerospace Sci., **32** (5), 457 (1996). DOI: 10.1016/0376-0421(95)00012-7
[8] T. Ota. Appl. Mech. Rev., **53** (8), 219 (2000). DOI: 10.1115/1.3097351
[9] V.I. Terekhov. Energies, **14** (4), 1005 (2021). DOI: 10.3390/en14041005
[10] W.D. Moss, S. Baker. Aero Quart., **31** (3), 151 (1980). DOI: 10.1017/S0001925900008878
[11] M. Raisee, S.H. Hejazi. Int. J. Heat Fluid Flow, **28** (3), 429 (2007). DOI: 10.1016/j.ijheatfluidflow.2006.07.004
[12] A. Graziani, M. Lippert, D. Uystepruyst, L. Keirsbulck. Int. J. Heat Fluid Flow, **67**, part A, 220 (2017). DOI: 10.1016/j.ijheatfluidflow.2017.08.009
[13] K. Hishida, T. Nagayasu, M. Maeda. Int. J. Heat Mass Transfer, **38** (10) 1773 (1995). DOI: 10.1016/0017-9310(94)00308-I
[14] M.A. Pakhomov, V.I. Terekhov. Water, **13** (17), 2333, (2021). DOI: 10.3390/w13172333
[15] K.-T. Huang, Y.-H. Liu. Energies, **12** (19), Paper 3785 (2019). DOI: 10.3390/en12193785

[16] M.A. Pakhomov, V.I. Terekhov. Flow, Turbulence, Combust., **98** (1), 341 (2017). DOI: 10.1007/s10494-016-9732-7
[17] M.A. Pakhomov, V.I. Terekhov. Tech. Phys., **58** (2), 185 (2013). DOI: 10.1134/S1063784213020187
[18] M.A. Pakhomov, V.I. Terekhov. Pisma v ZhTF,**49** (7), 16 (2023) (in Russian).
[19] L.I. Zaichik. Phys. Fluids, **11**(6), 1521 (1999). DOI: 10.1063/1.870015
[20] R.V. Mukin, L.I. Zaichik. Int. J. Heat Fluid Flow, **33** (1), 81 (2012). DOI: 10.1016/j.ijheatfluidflow.2011.11.002
[21] A. Fadai-Ghotbi, R. Manceau, J. Boree. Flow, Turbulence Combust., **81** (3) 395 (2008). DOI: 10.1007/s10494-008-9140-8
[22] N. Beishuizen, B. Naud, D. Roekaerts. Flow, Turbulence Combust., **79** (3), 321 (2007). DOI: 10.1007/s10494-007-9090-6
[23] B.P. Leonard. Comput. Methods Appl. Mech. Eng., **19** (1), 59 (1979). DOI: 10.1016/0045-7825(79)90034-3
[24] J.P. Van Doormaal, G.D. Raithby. Numer. Heat Transfer, pt. A, **7** (2), 147 (1984). DOI: 10.1080/01495728408961817
[25] J.R. Fessler, J.K. Eaton. J. Fluid Mech., **314**, 97 (1999). DOI: 10.1017/S0022112099005741
[26] Y.H. Wu, H.Y. Ren. Phys. Fluids, **23** (4), 045102 (2011). DOI: 10.1063/1.3576911
[27] X.J. Fang, M.F. Tachie, D.J. Bergstrom. Int. J. Heat Fluid Flow, **87**, 108753 (2021). DOI: 10.1016/j.ijheatfluidflow.2020.108753

Translated by I.Mazurov